Colloids and Surfaces A: Physicochemical and Engineering Aspects 738 (2026) 140054

Contents lists available at ScienceDirect

Colloids and Surfaces A: Physicochemical and Engineering Aspects

journal homepage: www.elsevier.com/locate/colsurfa

Robust and fluorine-free: A photothermal superhydrophobic coating for synergistic passive and active deicing

Shujun Liu [a,b,1], Quan Yan [a,1], Yue Gui [a], Xinlu Xiao [a], Jie Zhou [a], Huixuan Peng [d,*], Haitao Yang [a,c,**]

[a] School of Materials Science and Engineering, Nanchang Hangkong University, Nanchang 330063, China
[b] Jiangxi Provincial Key Laboratory of Lightweight Composite Materials, Nanchang 330063, China
[c] State Key Laboratory of Molecular Engineering of Polymers (Fudan University) 200438, China
[d] School of Intelligent Manufacturing and Materials Engineering, Gannan University of Science and Technology, Ganzhou 341000, China

GRAPHICAL ABSTRACT

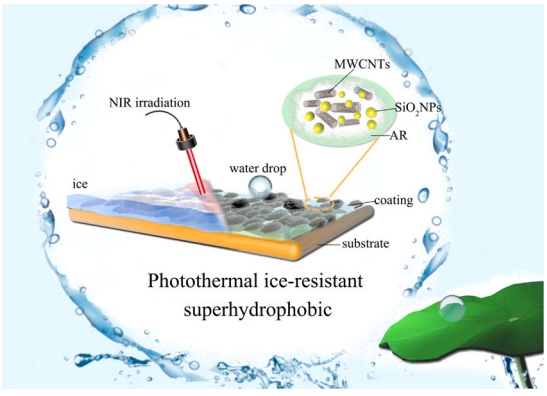

ARTICLE INFO

Keywords:
Photothermal effect
Superhydrophobic surface
Fluorine-free coating
Nanocomposites
De-icing

ABSTRACT

Superhydrophobic coatings, as a passive de-icing strategy, hold great promise for addressing the significant economic losses and safety issues caused by icing. However, conventional superhydrophobic materials often suffer from low de-icing efficiency, high energy consumption, and reliance on environmentally harmful fluorinated compounds. In this study, we developed a novel robust and fluorine-free anti-icing coating with high photothermal conversion efficiency by depositing a mixture of carbon nanotubes (CNTs), hydrophobic silica (SiO_2) nanoparticles, and an adhesive acrylate polymer resin onto an aluminum substrate. The optimized composite coating features a micro/nano-roughness of 3.34 μm, exhibiting excellent superhydrophobicity with a water contact angle of 165° and a sliding angle of 6.5°. Through the synergistic effect of passive anti-icing and active photothermal de-icing, the coating prolongs the water freezing time by 377 s and significantly reduces ice adhesion strength to 36.9 kPa. Most importantly, under near-infrared irradiation, the surface temperature can

* Corresponding author.
** Corresponding author at:School of Materials Science and Engineering, Nanchang Hangkong University, Nanchang 330063, China.
E-mail addresses: phx12829@163.com (H. Peng), yht@nchu.edu.cn (H. Yang).
[1] S.L. and Q.Y. contributed equally to this work.

https://doi.org/10.1016/j.colsurfa.2026.140054
Received 26 December 2025; Received in revised form 2 February 2026; Accepted 21 February 2026
Available online 22 February 2026

rapidly rise to 90 ℃, achieving complete de-icing within 8 s in an outdoor environment. The demonstrated durability, eco-friendliness, and high efficiency suggest a broad range of potential applications for this coating in aviation and power transmission.

1. Introduction

The accumulation of ice and snow is a natural phenomenon that can lead to severe consequences across various sectors, including aviation [1,2], power transmission [3,4], wind power generation [5], and agricultural production [6]. For instance, the catastrophic snowstorm in Texas significantly impacted personal safety and economic stability [7]. Consequently, developing safe and efficient de-icing strategies is of paramount importance. Traditional active de-icing methods, such as mechanical scraping [8], electro-thermal heating [9], and chemical fluids [10], are widely used but often criticized for their high energy consumption, environmental pollution, and limited applicability in remote areas.

Inspired by the lotus leaf, superhydrophobic coatings have emerged as a promising **passive anti-icing strategy**. These surfaces utilize micro/nano-roughness to trap air pockets, minimizing the contact area between water droplets and the substrate, thereby reducing ice adhesion [11–14]. However, in harsh environments (e.g., high humidity or extremely low temperatures), passive surfaces alone may fail due to frost accumulation or mechanical interlocking of ice. To overcome this limitation, integrating **active photothermal de-icing** capability into superhydrophobic coatings has attracted considerable attention [15,16]. Carbon nanotubes (CNTs), known for their exceptional photothermal conversion efficiency, are widely employed in this regard. For example, recent studies have successfully combined CNTs with various polymers to create coatings that generate heat under sunlight or near-infrared (NIR) irradiation [17–20].

Despite these advancements, **two critical challenges remain**. First, to achieve low surface energy, most existing photothermal superhydrophobic coatings heavily rely on **fluorinated polymers** or fluorosilanes [17,19]. These fluorinated compounds are expensive and pose potential risks to human health and the environment due to their persistence and toxicity. Second, constructing a **robust** hierarchical structure is difficult; many superhydrophobic surfaces are mechanically fragile and easily lose their anti-icing function under abrasion or wear [12,21]. Therefore, developing a coating that simultaneously achieves **fluorine-free eco-friendliness, mechanical robustness, and high photothermal efficiency** remains a significant challenge.

Addressing these issues, we propose a facile spray-coating strategy to fabricate a **robust and fluorine-free** photothermal superhydrophobic coating for synergistic passive and active de-icing. We synthesized a specialized acrylate copolymer resin (AR) as a robust binder and combined it with multi-walled carbon nanotubes (CNTs) and hydrophobic silica (SiO_2) nanoparticles. The resulting composite coating features a stable micro/nano-structure that creates an effective barrier against water and ice. **Distinct from conventional fluorinated coatings**, our design utilizes eco-friendly materials while maintaining excellent water repellency (WCA∼165°) and wear resistance. Under NIR irradiation, the coating demonstrates rapid photothermal response, enabling efficient de-icing in outdoor environments. This work provides a sustainable and durable solution for anti-icing applications in aviation and power infrastructure. (Fig. 1)

2. Experimental section

In a 250 mL four-neck flask, add tetrahydrofuran (THF) (30 g), and adjust the reaction temperature to 69 °C. Prepare a mixed solution of acrylic acid (AA), methyl acrylate (MMA), butyl acrylate (BA), THF, and the initiator azobisisobutyronitrile (AIBN), then ultrasonically homogenize to obtain a uniform mixture and transfer it to a constant-pressure addition funnel. After the monomer mixture is purged with nitrogen for 5 min, begin the dropwise addition. The mass ratio of AA, MMA, and BA is 15:5:6, and the AIBN addition amount is 5 % of the total mass of AA, MMA, and BA. Real-time monitoring of the reaction progress is performed by FTIR sampling, and the reaction ends after 8 h. The synthesized copolymer is purified with hexane twice, then placed in an oven at

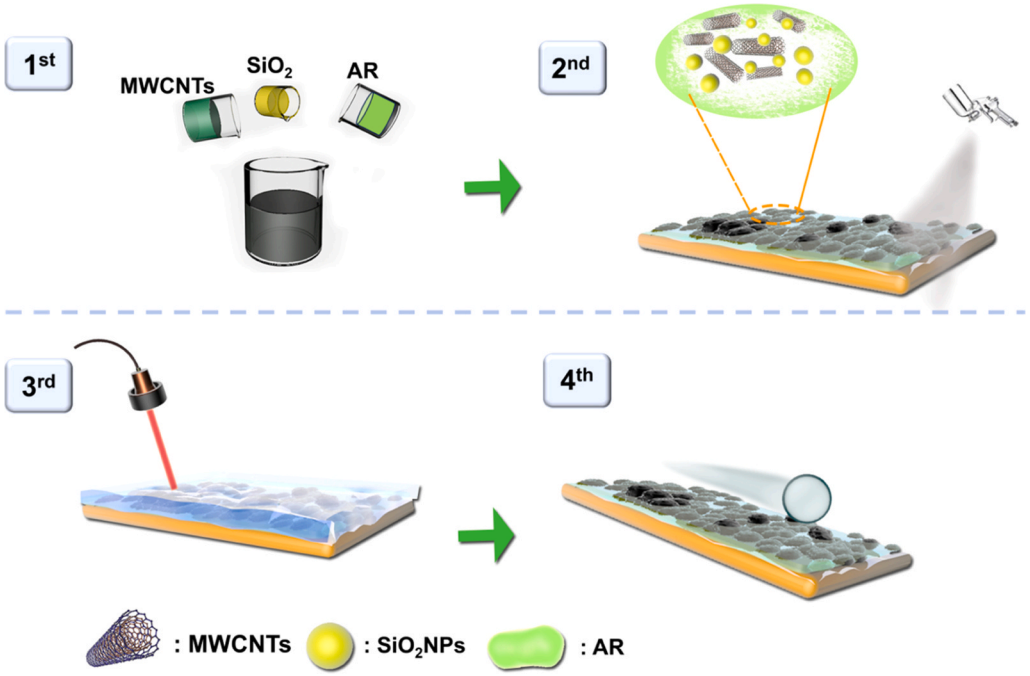

Fig. 1. Preparation process of the coating.

60 °C. to dry for 12 h and kept aside for future use. AR (0.5 g), CNTs (0.02 g), SiO_2 (0.3 g), and Hexadecyltrimethoxysilane (HDTMS, 0.1 g) were then dissolved in ethanol and sonicated for 30 min. The coating, labeled ACSH15, was prepared by spray-coated the suspension onto a 30 mm*30 mm aluminum sheet. For comparison study, the control samples including AR/SiO_2, AR/CNTs and AR, were also prepared. Additionally, coatings were fabricated using CNTs and SiO_2 in mass ratios of 1:5, 1:10, 1:20, and 1:25, following the aforementioned method (the mass ratio of CNTs and SiO_2 were 1:5, 1:10, 1:15, 1:20, 1:25, named as ACSH5, ACSH10, ACSH15, ACSH20, ACSH25). Figure. S1 displays the typical fourier transform infrared (FT-IR) spectrum of the synthesized AR. The absorption peaks at 2960 cm^{-1} and 2875 cm^{-1} correspond to the antisymmetric and symmetric stretching vibrations of -CH_2- [22]. The strong band near 1760 cm^{-1} is assigned to the -C═O stretching vibration of ester groups present in the polymerized acrylic resin (MMA and BA units) formed during AR resin synthesis [23]. The absence of a -C═C- absorption peak at 1640 cm^{-1} after 6 h of reaction indicates the successful AR synthesis [24].

3. Results and discussion

3.1. Surface morphology and wettability

The microscopic morphology of the coatings with different component ratios is illustrated in Fig. 2. The surface sprayed with pure AR resin appears flat and smooth (Fig. 2**a**). The pristine SiO_2 nanoparticles exhibit good particle size uniformity and dispersion (Figure S2). With the incorporation of SiO_2, a distinct rough micro/nano-structure emerges due to the synergistic assembly of CNTs and SiO_2 (Figure. S3). Specifically, for the ACSH15 sample, the particles are uniformly dispersed, forming a hierarchical villous structure (Fig. 2**b**). However, when the SiO_2 content is further increased to a ratio of 1:25, severe

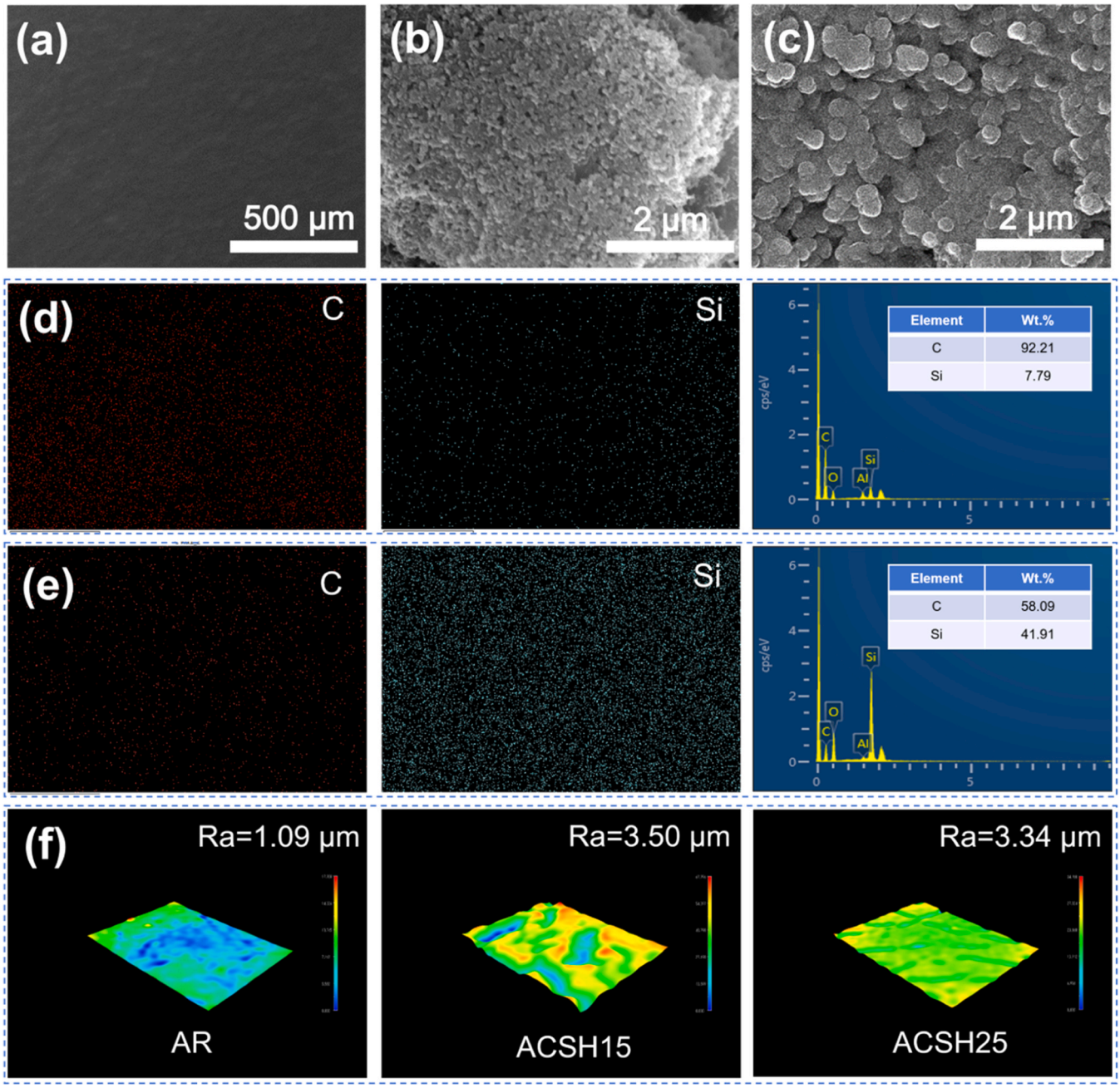

Fig. 2. (a-c) SEM images of AR, ACSH15 and ACSH25 coatings. (d-e) EDS images of ACSH5 and ACSH25. (f) 3D images of different samples.

particle agglomeration is observed (Fig. 2**c**).

Energy-dispersive X-ray spectroscopy (EDS) analysis confirms the composition changes (**Figures. 2d, e, and S4**). The silicon (Si) content on the surface increases from 7.79 wt% to 41.91 wt% with the addition of SiO_2, which aligns well with the SEM observations. Furthermore, 3D profilometry reveals that while the AR sample is relatively flat, the composite coatings exhibit numerous gully-like protrusions. The surface roughness (Ra) increases from 1.09 μm to 3.98 μm as the particle concentration rises (Fig. 2**f and S5**). Notably, for the optimized ACSH15 coating, the dense coverage of nanoparticles results in a uniform surface with a roughness of 3.34 μm.

The wettability of the coatings was evaluated by measuring water contact angles (WCAs) and sliding angles (SAs), as shown in Fig. 3**a**. The bare aluminum, AR, and ACSH5 samples fail to achieve superhydrophobicity, exhibiting WCAs below 150°. In contrast, the ACSH15 sample demonstrates excellent superhydrophobicity with a high WCA of 165° and a low SA of 6.5°. This superior water repellency is attributed to the air pockets trapped within the stable hierarchical micro/nanostructure, which corresponds to the Cassie-Baxter state. As expected, further increasing the SiO_2 content (1:20 and 1:25) leads to a decrease in superhydrophobicity due to excessive agglomeration. Additionally, the hydrophobic SiO_2 nanoparticles used in this study are rendered hydrophobic through modification with long-chain organosilane molecules, without the incorporation of any fluorine-containing species (Figure S6), thereby enabling superhydrophobicity while avoiding potential environmental harm.

3.2. Durability and chemical stability

The durability of the coating is critical for practical applications. As shown in Fig. 3**b**, the ACSH15 coating exhibits outstanding chemical stability against various liquids, including acidic/alkaline solutions, soda, cola, milk, and tea. All droplets retain a spherical shape and slide off easily, confirming the coating's excellent self-cleaning ability.

Mechanical robustness was assessed via a tape-peeling test and an abrasion test. Thanks to the strong adhesion of the AR binder, the detached area of the ACSH15 coating after the tape-peeling test was less than 5 % (Fig. 3**c**), classifying it as Grade 0–1 standard. Moreover, the coating maintained its superhydrophobicity even after 10 cycles of abrasion under a 200 g load (Fig. 3**d**), with an average water contact angle (WCA) of 153.5°. Interestingly, although the WCA fluctuated slightly, the abrasion process exposed fresh micro/nano-rough structures, allowing the coating to sustain its high water repellency.

3.3. Passive anti-icing performance

The passive anti-icing performance was evaluated by measuring the freezing time of water droplets and ice adhesion strength at −10 °C. As shown in Fig. 4**a-c**, the water droplet on the bare Al substrate froze rapidly within 130 s. In contrast, the freezing time on the ACSH15 coating was significantly prolonged to **527 s**, which is nearly four times that of the Al substrate. This delay in freezing is attributed to the "air cushion" effect trapped within the superhydrophobic micro/nanostructure. This air layer acts as a thermal barrier, effectively reducing heat transfer between the water droplet and the cold substrate [25,26].

Furthermore, low ice adhesion is crucial for easy ice removal. Superhydrophobic micro/nanostructures reduce ice adhesion strength primarily by trapping air in their hierarchical roughness, which promotes the Cassie-Baxter wetting state. This state significantly decreases the real contact area between the ice and the surface. The fraction of the actual solid-liquid contact area at the bottom of the droplet relative to its projected base area is defined as ϕ. Consequently, the heterogeneous stress distribution and minimized solid-liquid interface facilitate crack initiation and ice detachment under external forces, leading to ultra-low ice adhesion [13]. Fig. 4**d** presents the ice adhesion strength (τ_{ice}) of different surfaces. The bare Al substrate exhibited a strong ice adhesion

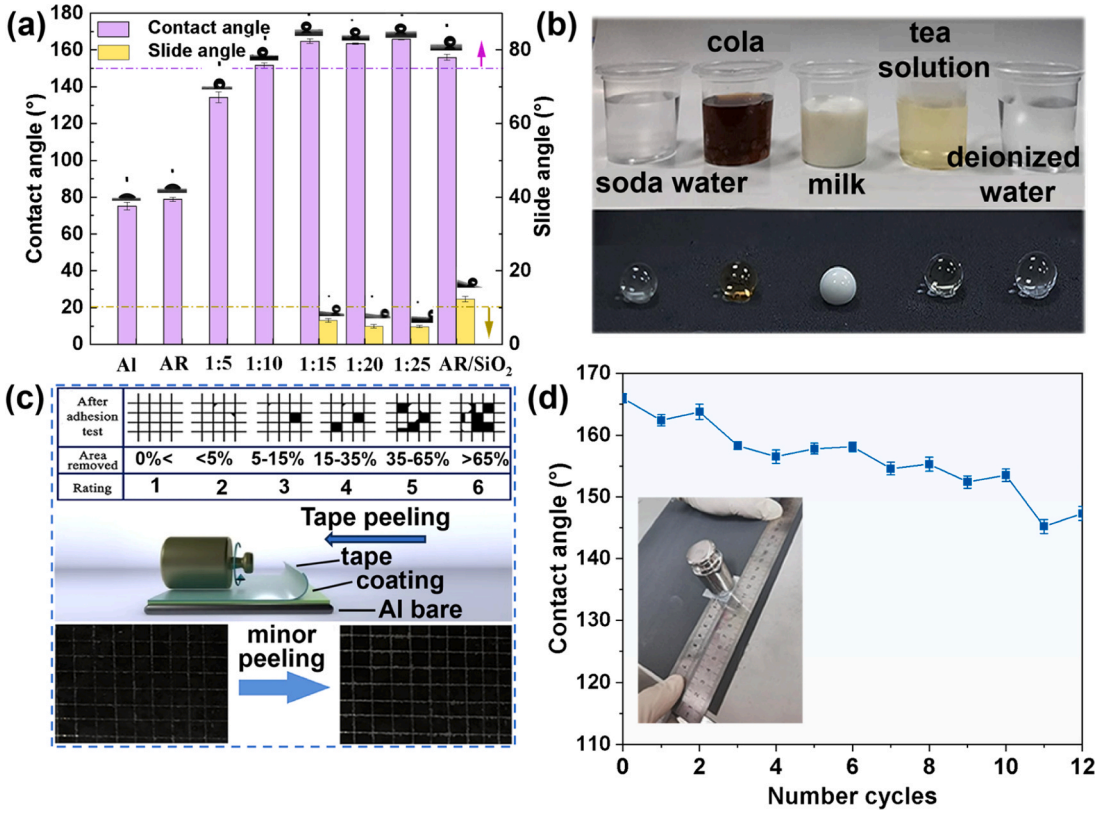

Fig. 3. (a) The contact angles and sliding angles of different samples. (b) Self-cleaning test of ACSH15. (c) Adhesion of ACSH15. (d) Contact angle of ACSH15 under different wear cycles.

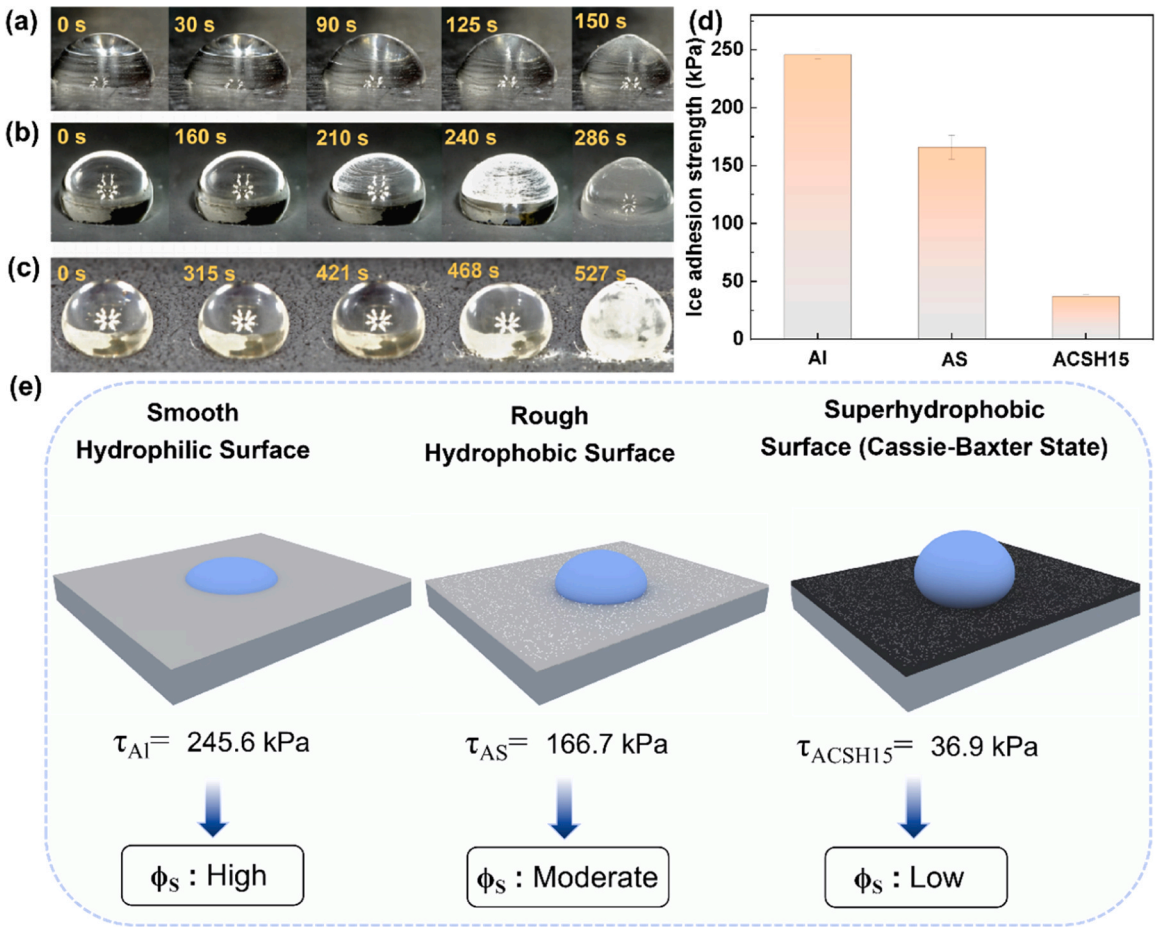

Fig. 4. The icing process of Al (a), AR/SiO_2 (b) and ACSH15 (c). (d) Ice adhesion strength of different samples. (e). Schematic diagram illustrating the ice adhesion mechanisms on different sample surfaces.

of 245.6 kPa due to the large contact area caused by its hydrophilic nature. The AR/SiO_2 coating reduced this value to 166.7 kPa. Remarkably, the ACSH15 coating demonstrated the lowest ice adhesion strength of only **36.9 kPa**, well below the threshold for passive ice shedding (100 kPa). The corresponding schematic illustration of the mechanism is shown in Fig. 4**e**. Based on established theoretical models and indirect experimental indicators, such as wettability, surface roughness, and macroscopic adhesion measurements (Figs. 2f, 3**a and** 4**d**), the ultra-low ice adhesion is generally attributed to the significantly reduced real contact area associated with the Cassie-Baxter wetting state, as well as the heterogeneous stress distribution at the ice-solid interface. Such interfacial characteristics have been widely reported to promote interfacial crack initiation and facilitate ice detachment under external perturbations [13,17,27].

3.4. *Active photothermal de-icing performance*

While passive thermal management strategies are effective, they may be insufficient under extreme conditions. To enhance de-icing performance, active photothermal capabilities were integrated into the coatings. As shown in Fig. 5**a**, under near-infrared (NIR) laser irradiation (808 nm, 2 W), the bare aluminum (AR) substrate exhibits minimal temperature rise, maintaining around 18 °C due to its high thermal conductivity but limited heat storage. The AR coating elevates the temperature to 48 °C, demonstrating the heat-storage ability of the resin. Incorporation of SiO_2 and CNTs further boosts photothermal response; the AR/SiO_2 coating reaches approximately 60 °C, while the AR/CNTs coating attains about 80 °C, indicating enhancements of 12 °C and 32 °C over the plain AR coating, respectively. The optimized ACSH15 coating achieves a steady-state temperature of 89.9 °C in just 210 s, reflecting the combined effects of the aluminum substrate's thermal conductivity, the heat-retention capacity of the resin matrix, and the dispersion state of SiO_2 and CNTs. In the photothermal de-icing experiment, we evaluate the photothermal energy utilization via a semi-quantitative energy-balance approach [18]. The calculated photothermal conversion efficiency for the ACSH15-coated sample is 48.9 %. The detailed calculation procedure and the corresponding experimental data are presented in the supplementary information and Figure S7**.**

The effect of component ratio on photothermal efficiency is detailed in Fig. 5**b**. The ACSH15 sample, with increased SiO_2, exhibits pronounced micro/nano-rough structure with more uniform nanoparticle dispersion, yielding a velvet-like micro/nano morphology (Fig. 2**b**). This morphology further enhances the surface's photothermal performance by increasing light trapping and absorption. However, excessive SiO_2 (e.g., 1:20 and 1:25 ratios) tends to cover the CNTs, impeding light absorption and reducing the equilibrium temperature. The cyclic stability of the ACSH15 coating was also tested (Fig. 5**c**). After six heating-cooling cycles, the peak temperature remained stable at approximately 90 °C, indicating excellent photothermal durability.

The practical de-icing capability was demonstrated through both laboratory and outdoor tests. In the laboratory defrosting test at −10 °C (Fig. 5**e**), the frost layer on the ACSH15 surface completely melted within 150 s under NIR irradiation. More impressively, in the de-icing test (Fig. 5**f**), the ice bead on the coating melted into water in just **26 s**, whereas the ice on the reference samples remained frozen.

Finally, to simulate real-world conditions, an outdoor de-icing test was conducted under natural sunlight at 15 °C (Fig. 5**g**). Due to the smooth surface of the bare Al substrate, the ice slipped off by gravity in

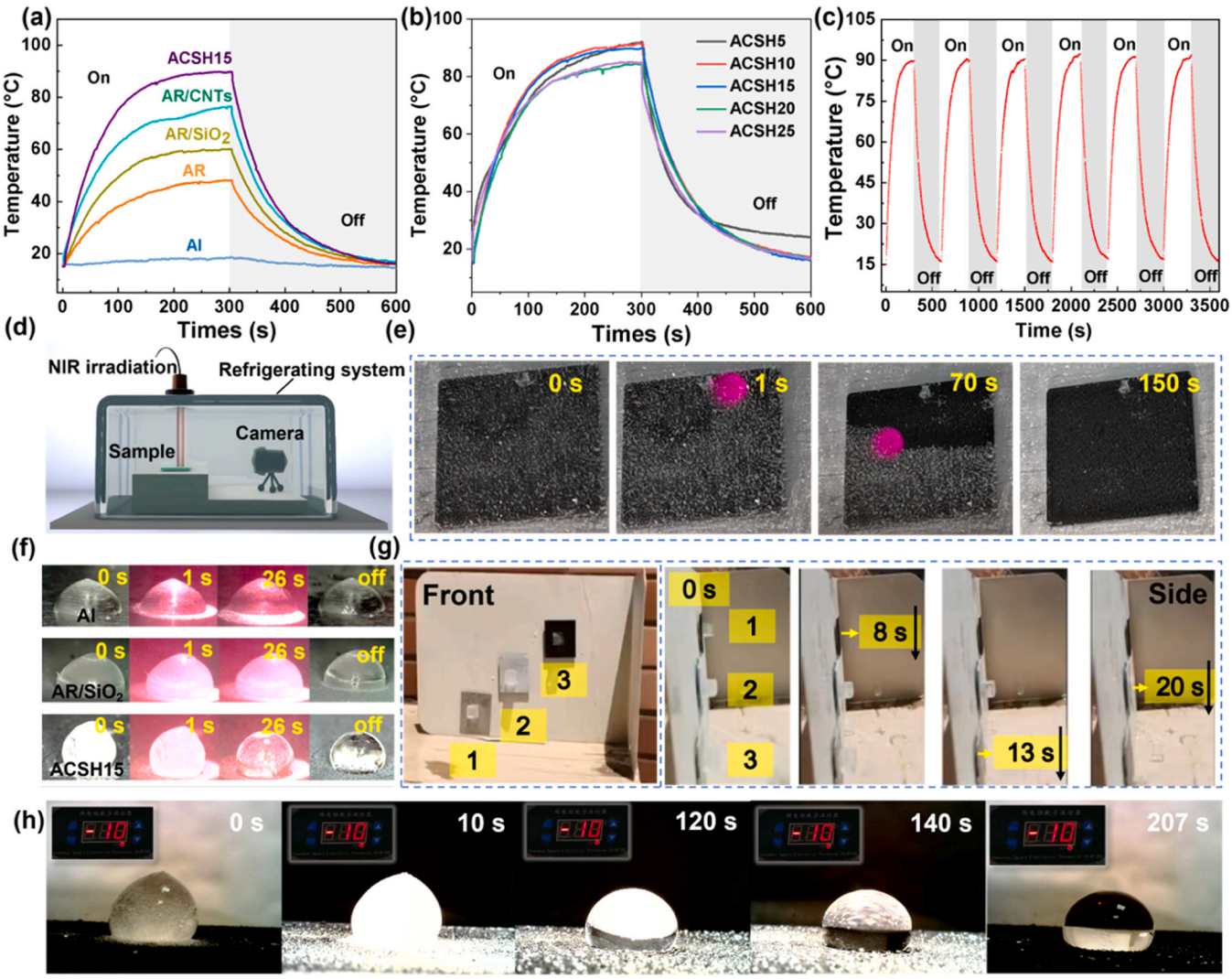

Fig. 5. (a-b) Equilibrium temperature of different samples irradiated by 2 W near infrared laser. (c) Cycle stability of ACSH15 under 2 W near infrared irradiation. (d) Lab-made equipment for defrosting and deicing. (e) Defrosting process. (f) Deicing process of Al bare, AR/SiO_2 and ACSH15. (g) Outdoor deicing test of ACSH15, Al bare and AR/SiO_2. (h) De-icing test of the ACSH15 sample at −10 ℃ under xenon-lamp–simulated sunlight (1sun).

13 s. However, the ACSH15 coating achieved the fastest de-icing performance, with the ice sliding off in just **8 s**. Table S1 compares our coating with recently reported photothermal superhydrophobic anti-icing coatings, and the results show that our sample exhibits excellent superhydrophobic anti-icing performance [18,19,21,28–34]. As shown in Fig. 5**h**, the de-icing behavior of the ACSH15 coating was further evaluated at −10 °C under xenon-lamp-simulated solar irradiation to mimic practical sunlight-driven conditions. After illumination, the ice on the ACSH15 surface began to melt rapidly from the ice-substrate interface, and a distinct water layer formed at 120 s, followed by complete melting at 207 s. This superior performance is attributed to the synergistic effect of the superhydrophobic interface (which reduces adhesion) and the photothermal heat generation (which creates a lubricating water layer at the interface). These results indicate that, even at subzero temperatures, the ACSH15 coating enables rapid and energy-efficient solar-driven de-icing, highlighting its strong potential for real-world outdoor anti-icing applications.

4. Conclusion

In summary, we have successfully developed a robust, fluorine-free, and high-efficiency photothermal superhydrophobic coating via a facile spray-coating method. By synergizing the photothermal conversion of CNTs, the roughness of SiO_2 nanoparticles, and the strong adhesion of acrylate resin, the composite coating exhibits excellent superhydrophobicity (WCA~165°) and mechanical durability. The coating demonstrates a dual-mode anti-icing mechanism: passively prolonging the water freezing time by 377 s and actively reducing ice adhesion strength to 36.9 kPa. Under NIR irradiation or sunlight, the surface temperature can rapidly rise to~90 °C, enabling ultrafast de-icing (8 s) in outdoor environments. This work provides an eco-friendly and scalable solution for ice protection in aviation, power transmission, and other industrial applications, offering a viable alternative to traditional fluorinated coatings. [14–16,20,21]

CRediT authorship contribution statement

Huixuan Peng: Visualization, Methodology, Investigation. **Quan Yan:** Methodology, Data curation. **Shujun Liu:** Writing – original draft, Methodology, Investigation, Formal analysis. **Haitao Yang:** Writing – review & editing, Supervision, Resources, Funding acquisition, Conceptualization. **Jie Zhou:** Validation. **Xinlu Xiao:** Methodology. **Yue Gui:** Formal analysis.

Declaration of Competing Interest

The authors declare that they have no known competing financial interests or personal relationships that could have appeared to influence the work reported in this paper.

Acknowledgements

This study was financially supported by Jiangxi Provincial Natural Science Foundation (No. 20232BAB214029), Jiangxi Provincial Key Laboratory of Lightweight Composite Materials (EJ202201353) and State Key Laboratory of Molecular Engineering of Polymers (Fudan University) (K2024–31).

Appendix A. Supporting information

Supplementary data associated with this article can be found in the online version at doi:10.1016/j.colsurfa.2026.140054.

Data availability

Data will be made available on request.

References

[1] J. Jiang, Y. Shen, Y. Xu, Z. Wang, J. Tao, S. Liu, W. Liu, H. Chen, An energy-free strategy to elevate anti-icing performance of superhydrophobic materials through interfacial airflow manipulation, Nat. Commun. 15 (2024) 777.
[2] L. Wang, X. Zhao, S. Li, S. Nie, J. Wang, J. Liu, Preventing ice accretion: design strategies for anti-icing surfaces, ACS nano 19 (2025) 36082–36105.
[3] X. Jiang, C. Fan, Y. Xie, New method of preventing ice disaster in power grid using expanded conductors in heavy icing area, IET Gener. Transm. Distrib. 13 (2019) 536–542.
[4] N. Zhao, X. Yu, K. Hou, X. Liu, Y. Mu, H. Jia, H. Wang, H. Wang, Full-time scale resilience enhancement framework for power transmission system under ice disasters, Int. J. Electr. Power Energy Syst. 126 (2021) 106609.
[5] W. Yao, Y. Ma, F. Chen, Z. Xiao, Z. Shu, L. Chen, W. Xiao, J. Liu, L. Jiang, S. Zhang, Analysis of ice storm impact on and post-disaster recovery of typical subtropical forests in southeast China, Remote Sens. 12 (2020) 164.
[6] S.S. Ray, R. Soni, I.-C. Kim, Y.-I. Park, C.Y. Lee, Y.-N. Kwon, Surface innovation for fabrication of superhydrophobic sand grains with improved water holding capacity for various environmental applications, Environ. Technol. Innov. 28 (2022) 102849.
[7] J. Doss-Gollin, D.J. Farnham, U. Lall, V. Modi, How unprecedented was the February 2021 Texas cold snap? Environ. Res. Lett. 16 (2021) 064056.
[8] Y. Zhang, L. Zhang, G. Luo, Study on de-icing criterion of anti-icing coating and simulation analysis method of mechanical de-icing process for polar ship superstructure, Ocean Eng. 288 (2023) 115811.
[9] Z. Zhao, H. Chen, X. Liu, Z. Wang, Y. Zhu, Y. Zhou, Novel sandwich structural electric heating coating for anti-icing/de-icing on complex surfaces, Surf. Coat. Technol. 404 (2020) 126489.
[10] W. Dong, J. Zhu, M. Zheng, G. Lei, Z. Zhou, Experimental study on icing and anti-icing characteristics of engine inlet guide vanes, J. Propuls. Power 31 (2015) 1330–1337.
[11] A.M. Emelyanenko, L.B. Boinovich, A.A. Bezdomnikov, E.V. Chulkova, K. A. Emelyanenko, Reinforced superhydrophobic coating on silicone rubber for longstanding anti-icing performance in severe conditions, ACS Appl. Mater. Interfaces 9 (2017) 24210–24219.
[12] H. Chen, F. Wang, H. Fan, R. Hong, W. Li, Construction of MOF-based superhydrophobic composite coating with excellent abrasion resistance and durability for self-cleaning, corrosion resistance, anti-icing, and loading-increasing research, Chem. Eng. J. 408 (2021) 127343.
[13] M.J. Kreder, J. Alvarenga, P. Kim, J. Aizenberg, Design of anti-icing surfaces: smooth, textured or slippery? Nat. Rev. Mater. 1 (2016) 1–15.
[14] Y. Meng, S. Xing, N. Wu, P. Zhang, X. Cui, X. Liang, S. Wang, Holistic anti/dewetting design of anti/deicing superhydrophobic surfaces (ADISS), ACS Mater. Lett. 6 (2024) 1457–1466.
[15] J. Zhang, P. Zhang, J. Liu, R. Zhang, W. Lin, X. Cui, B. Yan, Environmentally robust photothermal superhydrophobic coatings via a composition-interface synergistic reinforcement strategy for ultralow-temperature anti/de-icing, J. Mater. Sci. Technol. 263 (2026) 117–128.
[16] C. Shen, X. Qiu, P. Zhang, J. Liu, Z. Zhang, B. Dong, H. Liu, C. Huang, J. Huang, X. Cui, A supramolecular polydimethysiloxane-based coating with tunable surface topography for photothermal-enhanced sterilization, self-healing and anti/de-icing, Chem. Eng. J. 504 (2025), 158709-158709.
[17] K. Li, S. Xu, J. Chen, Q. Zhang, Y. Zhang, D. Cui, X. Zhou, J. Wang, Y. Song, Viscosity of interfacial water regulates ice nucleation, Appl. Phys. Lett. 104 (2014).
[18] G. Jiang, L. Chen, S. Zhang, H. Huang, Superhydrophobic SiC/CNTs coatings with photothermal deicing and passive anti-icing properties, ACS Appl. Mater. Interfaces 10 (2018) 36505–36511.
[19] Y. Liu, R. Guo, J. Liu, Q. Zhang, Robust PFMA/CNTs composite PDMS superhydrophobic film via SI-CuCRP method for efficient anti-icing, Colloids Surf. A Physicochem. Eng. Asp. 660 (2023) 130913.
[20] J. Zhang, P. Zhang, Z. Hu, C. Li, X. Cui, B. Yan, A fluorinated MXene-doped superhydrophobic coating with mechanochemical robustness, repairable wettability and photothermal conversion for highly efficient anti/de-icing, Chem. Eng. J. 498 (2024), 155499-155499.
[21] W. Binrui, C. Xin, J. Huayang, W. Nan, P. Chaoyi, H. Zhenfeng, L. Xiubing, Y. Yonggan, H. Jun, L. Diansen, A superhydrophobic coating harvesting mechanical robustness, passive anti-icing and active de-icing performances, J. Colloid Interface Sci. 590 (2021) 301–310.
[22] K. Jin, M. Zhang, J. Wang, Z. Jin, J. Sun, Y. Zhao, K. Xie, Z. Cai, Robust highly conductive fabric with fluorine-free healable superhydrophobicity for the efficient deicing of outdoor's equipment, Colloids Surf. A Physicochem. Eng. Asp. 651 (2022) 129639.
[23] K. Ding, J. Liu, H. Chen, H. Wang, Hyper-branched acrylic resin with high solid contents, J. Thermoplast. Compos. Mater. 31 (2018) 1149–1160.
[24] G. Chen, S. Liu, S. Chen, Z. Qi, FTIR spectra, thermal properties, and dispersibility of a polystyrene/montmorillonite nanocomposite, Macromol. Chem. Phys. 202 (2001) 1189–1193.
[25] Z. He, E.T. Vågenes, C. Delabahan, J. He, Z. Zhang, Room temperature characteristics of polymer-based low ice adhesion surfaces, Sci. Rep. 7 (2017) 42181.
[26] J. Lv, Y. Song, L. Jiang, J. Wang, Bio-inspired strategies for anti-icing, ACS nano 8 (2014) 3152–3169.
[27] Q. Yang, S. Au, Z.A. Dijvejin, K.A. Zarasvand, A. Dolatabadi, K. Golovin, Superhydrophobic surfaces exhibiting low interfacial toughness with ice, Chem. Eng. J. 508 (2025) 160929.
[28] S. Li, X. Liu, C. Xing, Y. Tan, A. Xiao, Y. Wei, C. Li, M. Dai, Preparation of superhydrophobic photothermal coatings via sequentially grown mesoporous silica-coated CNTs for anti-icing applications on cement concrete, J. Build. Eng. 105 (2025) 112449.
[29] Z. Liu, J. Hu, G. Jiang, Superhydrophobic and photothermal deicing composite coating with self-healing and anti-corrosion for anti-icing applications, Surf. Coat. Technol. 444 (2022) 128668.
[30] J. Wei, X. Wei, M. Hou, J. Wang, Fluorine-free photothermal superhydrophobic copper oxide micro-/nanostructured coatings for anti-icing/de-icing applications, ACS Appl. Nano Mater. 6 (2023) 9928–9938.
[31] C. Peng, D. Yang, Z. You, D. Ruan, P. Guan, Z. Ye, Y. Ning, N. Zhao, F. Yang, A photothermal and superhydrophobic emulsified asphalt coating modified by CNTs and PTFE for anti-icing and de-icing applications, Constr. Build. Mater. 416 (2024) 135148.
[32] T.N. Lo, I. Park, Photothermal superhydrophobic coatings based on wrinkled mesoporous carbon for efficient anti-icing and deicing, Carbon 243 (2025) 120496.
[33] X. Yang, Y. Liu, Y. Zhong, H. Chen, Anti/de-icing superhydrophobic coating with durability and self-healing by infiltrating photothermal self-stratifying organic layers into plasma-sprayed porous Al2O3–13% TiO2 underlayer, Surf. Interfaces 54 (2024) 105305.
[34] X. Liu, S. Li, Y. Wu, T. Guo, J. Xie, J. Tao, L. Dong, Q. Ran, Robust all-waterborne superhydrophobic coating with photothermal deicing and passive anti-icing properties, ACS Appl. Mater. Interfaces 15 (2023) 44305–44313.